MARTINI-based simulation method for step-growth polymerization and its analysis by size exclusion characterization

PCCP

PAPER

View Article Online
View Journal | View Issue

Cite this: *Phys. Chem. Chem. Phys.*, 2019, **21**, 21603

MARTINI-based simulation method for step-growth polymerization and its analysis by size exclusion characterization: a case study of cross-linked polyurethane†

Hassan Ghermezcheshme,[a] Hesam Makki,[a] Mohsen Mohseni,*[a] Morteza Ebrahimi[a] and Gijsbertus de With[b]

Received 17th June 2019,
Accepted 13th September 2019

DOI: 10.1039/c9cp03407b

rsc.li/pccp

Simulation studies of step-growth polymerization, *e.g.*, polymerization of polyurethane systems, hold great promise due to having complete control over the reaction conditions and being able to perform an in-depth analysis of network structures. In this work, we developed a (completely automated) simulation method based on a coarse-grained (CG) methodology, *i.e.*, the MARTINI model, to study the cross-linking reaction of a diol, a tri-isocyanate molecule and one-hydroxyl functional molecule to form a polyurethane network without and with dangling chains. This method is capable of simulating the cross-linking reactions not only up to very high conversions, but also under rather complicated reaction conditions, *i.e.*, a non-stoichiometric ratio of the reactants, solvent evaporation and multi-step addition of the reactants. We introduced a novel network analysis, similar to size-exclusion chromatography based on graph theory, to study the growth of the network during the polymerization process. By combining the reaction simulations with these analysis methods, a set of correlations between the reaction conditions, reaction mechanisms and final network structure and properties is revealed. For instance, a two-step addition of materials for the reaction, *i.e.*, first the dangling chain to the tri-isocyanate and then the diol, leads to the highest integrated network structure. We observed that different reaction conditions lead to different glass transition temperatures (T_g) of the network due to the distinct differences in the final network structures obtained. For example, by addition of dangling chains to the network, the T_g decreases as compared to the network without dangling chains, as also is commonly observed experimentally.

1. Introduction

Polyurethanes (PUs) are one of the important types of industrial polymers with properties that make them a suitable choice in different fields such as foams and composites,[1] sealants,[2] coatings,[3] hydrogels,[4] contact lenses, and medical devices.[5] The wide range of raw materials, and the molecular weight of different components as well as their ratio and functionality (OH and NCO) result in a versatile tool to design polymeric systems suitable for the abovementioned applications. In fact, a 3D cross-linked PU system can be realized by employing materials with an average functionality of more than 2. It is also possible to incorporate a component with one hydroxyl group to build up a network with dangling chains, which has the benefit of faster dynamics as compared to polymer chains connected from both sides to the network. These dangling chains can give desirable characteristics to the PU networks, such as being easy-to-clean, anti-fouling[6] and low lubricity.[7] However, the addition of dangling chains to PU systems may deteriorate the physical and mechanical properties of the material due to reasons such as introducing inhomogeneity to the network structure and leaving unreacted chains in the system. Moreover, the morphology of a cross-linked PU system combining hard and soft domains can significantly influence the properties of the network. A great deal of experimental work has been devoted to investigating the morphology of PU systems through different analysis methods, *e.g.*, scattering,[8] thermo-mechanical,[9] and scanning probe microscopy techniques.[10] In parallel, a considerable number of molecular dynamics (MD)

[a] *Department of Polymer and Color Engineering, Amirkabir University of Technology, 424 Hafez Ave., Tehran, Iran. E-mail: mmohseni@aut.ac.ir, hmakki@aut.ac.ir; Tel: +9821 6454 2434, +9821 6454 2441*

[b] *Laboratory of Physical Chemistry, Department of Chemical Engineering & Chemistry, Eindhoven University of Technology, POB 513, NL-5600 MB Eindhoven, The Netherlands*

† Electronic supplementary information (ESI) available: Atomistic and CG parameterization, T_g calculations, MSD as a function of conversion, and phase separation analysis. See DOI: 10.1039/c9cp03407b

simulation studies has been performed to give complementary insights into the matter.[11–19] In fact, molecular simulation is a powerful tool to investigate the details of molecular structures in a systematic and controlled way as it can provide us with valuable information which experimental techniques, at present, are unable to address.[20] It is worth emphasizing that simulation paves the way for "real-time" network characterization because one can study the evolution of the network structure at any stage of a polymerization, which is not always possible experimentally.

For a 3D network, generating a reliable structure is a major challenge. Note that most of the MD packages are not capable of simulating chemical reactions. Nevertheless, a considerable amount of research work has been performed to establish a robust method for developing reliable network structures for thermoset polymers. The vast majority of them, however, have been carried out for curing of epoxy resins with amine-type hardeners[21–36] and fewer focused on other cross-linked systems such as polyurethanes,[12–15] poly(dimethylsiloxanes),[37] poly(methacrylates),[38] polystyrenes,[39] phthalonitrile resins,[40,41] bismaleimide resins[42] and polyesters with melamine hardeners.[43] These simulations have been performed at both the atomistic and CG level. In the case of cross-linking reactions, it is of great importance to cover sufficiently long reaction times. This provides priority of CG methods for such study, as is reflected in a considerably larger number of research studies that preferred CG models over atomistic ones.[34,36,43–47]

Different methodologies have been developed to realize a cross-linked polymeric network. As one of the first, Grest and Kremer[48] generated randomly a cross-linked network by a bead-spring model and investigated the static properties of the network. Analysis of the average strand length between cross-links and the distribution of strand lengths showed that the generated network was rather homogeneous. Some researchers used a Lennard-Jones potential to keep reactant moieties close together after a reaction has taken place. For instance, Nouri and Ziaei-Rad[28] presented a new algorithm to simulate the cross-linking process of an epoxy network. The reaction between functional groups was simulated using a Lennard-Jones 12-6 potential with modified σ and ε to keep the active C and N atoms together without "real" bond formation. To avoid having a reaction between more than two active C atoms with an active N atom, an unrealistic repulsive force between active C–C atoms was defined. Nevertheless, under realistic conditions, some bonds are broken and new bonds are formed as a result of cross-linking; therefore, to make more reliable network structures, creating "real" chemical bonds between active atoms seems necessary. Lin and Khare[49] used an annealing algorithm to find reactive atoms which are sufficiently close together. They cross-linked an epoxy-based system by this algorithm in a single-step polymerization process. They stated that bond formations by single-step polymerization results in high-energy penalties to the polymeric network, so that after all bonds were formed, they performed a single energy minimization step to relax the system towards the thermodynamic equilibrium state. To move one more step closer towards real conditions, one needs to define a certain cut-off distance for the chemical moieties that potentially can react. Heine *et al.*[37] simulated end-linked poly(dimethylsiloxane) networks at the atomistic level using a united atom force-field. They defined a reaction radius cut-off of 6.5 Å. The cross-linking procedure was done dynamically so that the potential of a newly formed bond is defined by using an adjusted potential, *i.e.*, a harmonic potential below the cut-off value and linear potential at a radius larger than the cut-off. The method of relaxing the network after cross-linking has taken place has been improved by several scientists. For instance, Varshney *et al.*[30] developed a relaxation method by defining different cross-linking approaches.

Gavrilov *et al.*[36] presented a multi-scale method to generate an epoxy-based polymeric network. They used dissipative particle dynamics (DPD) to simulate chemical reactions. Bond formation between linkers (active sites) occurs when their distance reaches a defined length (R_c) for bond formation. Iype *et al.*[15] studied polyurethane networks with and without hydrophilic dangling chains by means of a simulation approach based on the DPD method. Analyzing the cross-linked PU network through the radial distribution function and the cross-link point density distribution showed a homogeneous distribution of cross-linker molecules, but in the network containing dangling chains, phase separation of these chains was observed.

One of the effective coarse-graining models that is presented by Marrink *et al.*[50,51] is the MARTINI method. This method is a CG model developed initially for simulation of lipids and biomolecules and used for other molecules such as proteins,[52–54] carbohydrates,[55] DNA and RNA,[56,57] solvents,[58] polymers[59–61] and nanoparticles.[62] In the MARTINI approach, coarse-graining of atoms into beads is not uniquely defined and the numbers of heavy atoms assigned to a bead can be 2, 3 or 4. MARTINI beads are divided into four main types of interaction sites: polar (P), nonpolar (N), apolar (C), and charged (Q) and each main site is divided into different subtypes according to the polarity and ability to form a hydrogen bond. The ability of the MARTINI force field to distinguish between beads with hydrogen bond donor or hydrogen bond acceptor capacity makes this force field a suitable choice for simulation of polymeric systems, especially polyurethane. However, to the best of our knowledge, only one research study used the MARTINI model to simulate the cross-linking procedure of the polymeric network. Rossi *et al.*[43] presented a MARTINI-based model to simulate the cross-linking of a polyester resin with a melamine type hardener. The reaction between the hydroxyl groups of the polyester and the methoxy groups of the melamine hardener was modeled by defining an *ad hoc* potential between reactive beads. This potential was harmonic at distance below 5 Å and was smoothly switched to 0 kJ mol^{-1} between 5 and 6 Å by means of a fourth-order polynomial. Using their model the authors predicted the elastic modulus as a function of polymerization degree. By this procedure, the formation of bonds between hydroxyl groups and methoxy groups is not limited to one. Therefore, in this method more than one reacting site forms bonds with another reacting site. Moreover, the bead typing of reactants remained unchanged after the reaction occurs, although this assumption is fair for some cases, it cannot be accepted for the case of PU

systems due to the possibility of formation of hydrogen bonding of urethane moieties after a cross-linking reaction. Note that the *ad hoc* attractive potential between reacting sites might intensify this effect.

In the present work, we developed a method to mimic the cross-linking procedure of PU systems based on the MARTINI force field using the GROMACS simulation software package.[63] For cross-linking, chemical reactions between NCO and OH beads are simulated in a stepwise manner using a determined reaction cut-off distance. Note that all steps of a cross-linking procedure were carried out in an automated manner. This procedure is designed in a reasonably flexible manner so that one can generalize it for thermoplastic PUs as well as for any other condensation polymerizations such as the curing of epoxy/amine and, various polyester/melamine systems without spending considerable effort.

2. Method

We developed an efficient and reliable simulation method to form 3D PU networks. This method is based on the MARTINI model and is capable of mimicking real experimental parameters by which one can study the effect of several practical parameters on the final structure and properties of the network. As already mentioned, this method is fully automated and suitable for any kind of step-growth polymerization reaction. In this section, we introduce the algorithm of our method in detail. Note that most of the parameterization details are elaborated in the ESI.† Later on, we discuss the network analysis techniques that we developed and used.

2.1. Materials

We used polytetramethylene glycol, PTMG (M = 522 g mol^{-1}) as diol, methoxy-polyethylene glycol, mPEG (M = 516 g mol^{-1}) as hydrophilic dangling chain, HDI-based tri-isocyanate as cross-linker and *n*-butyl acetate (nBAc) as solvent, see Fig. 1, and the solid content is set around 60 wt% for all simulations.

2.2. Coarse-graining

In the MARTINI approach, coarse-graining of atoms into beads is not constant and the number of heavy atoms assigned to a bead can be 2, 3 or 4. The type that is assigned to a certain bead is based on the polarity and the ability of the bead to form a hydrogen bond. Our bead typing is illustrated in Fig. 1.

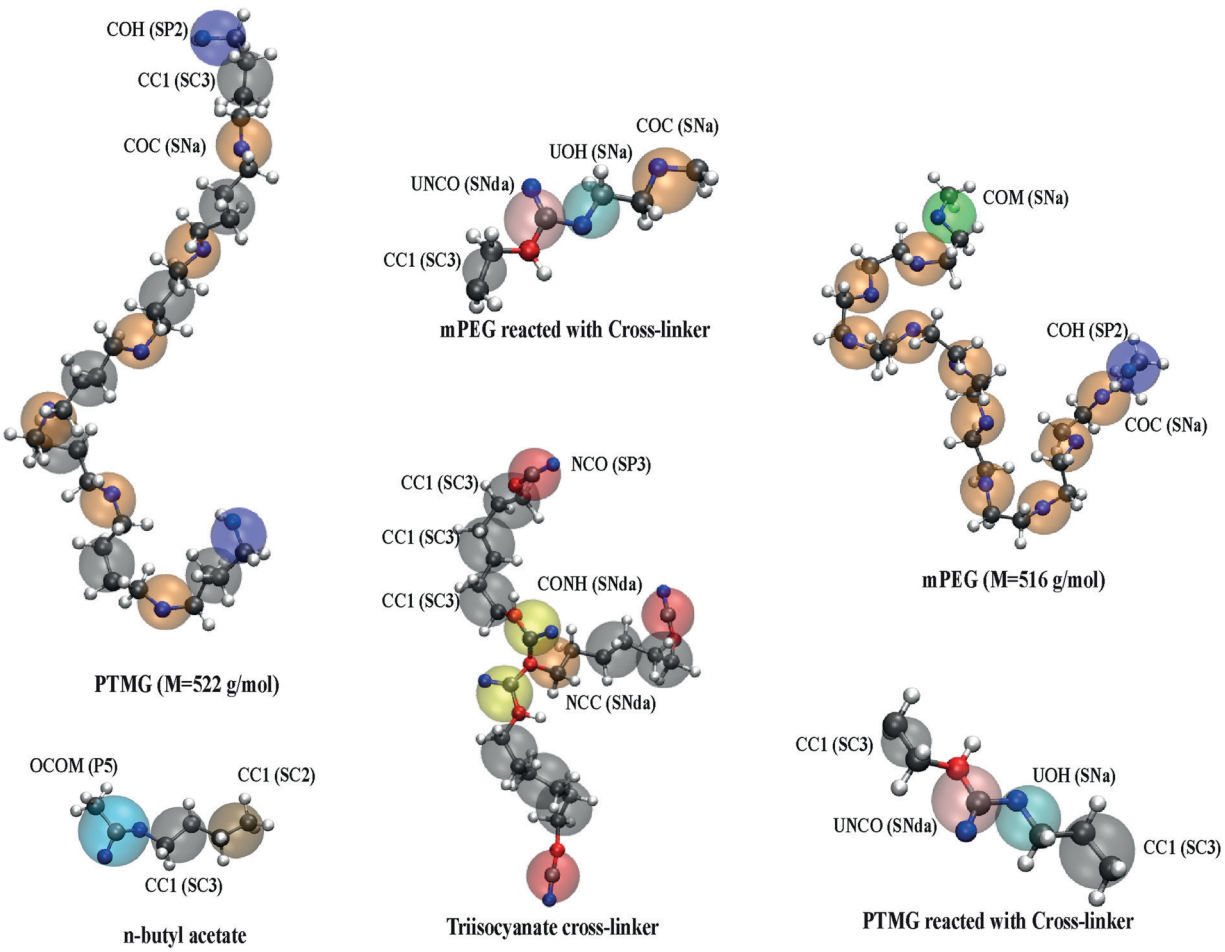

Fig. 1 CG mapping of the materials based on the MARTINI method. Our bead labeling is different to the MARTINI model. The corresponding MARTINI beads are mentioned in the brackets. Colors red, white, black and blue are assigned to nitrogen, hydrogen, carbon and oxygen atoms, respectively.

2.3. Parameterization

We, first, performed an atomistic-detailed simulation to fit the parameters to the CG model. The OPLS-AA force-field was used for the MD simulation at the atomistic level. To the best of our knowledge, there is no open source universal force field to cover all the parameters needed for our system of interest, in particular containing the bonded parameters of isocyanate and biuret groups. Therefore, only for these chemical moieties, we estimated the bonded parameters and converted them into OPLS-AA format, which we eventually used in the updated OPLS-AA force field to extract the CG parameters for all atoms. The effect of this inconsistency in the force field on the results is estimated to be small since the number of chemical moieties we treated differently is negligible as compared to the number of all chemical moieties in the system. Detailed information about the atomistic parameterization is given in the ESI,† Section S1. After obtaining all atomistic data, we calculated the bonded CG parameters by mapping from atomistic simulations for each material, and non-bonded MARTINI parameters are taken directly from original MARTINI parameters.[50] Butyl acetate in a non-aqueous medium does not dissociate to any large extent. Hence, charged moieties are absent and electrostatic interactions are neglected. Polarization effects may also be of importance for MARTINI simulations.[64–67] A set of simulations has been performed on the atomistic and CG levels. We drew a comparison between the real and simulated density of each material, see Table 1, to examine the accuracy of our parameterization at both levels. As shown, the real and simulated values show good agreements for all materials; therefore, we believe that parameterization on both levels is acceptable. The radius of gyration R_g and end-to-end distance R_{end} are reported in Table 1. As seen in Table 1, the R_g and R_{end} at atomistic and CG level are in good agreement. It is worth mentioning that for mPEG and PTMG we used only the bonded and non-bonded parameters of the OPLS-AA force field. Therefore, the similarity of R_g and R_{end} shows that parameterization in CG level is adequate. To verify further the applicability of the method, we also calculated the R_g and R_{end} for mPEG with n = 9 and 18 under similar conditions as for another published paper reported for PEO.[68] The results are very similar: R_gs at the CG level for n = 9 are 6.3 Å and 6.0 Å, and for n = 18 are 9.1 Å and 8.8 Å, for PEO and mPEG respectively.

2.4. Polymerization at the CG level

In this section, we briefly introduce the simulation procedure for the polymerization of a PU network by reacting OH and NCO groups of diol and tri-isocyanate, respectively. This method leads to the creation of a 3D cross-linked PU network. Fig. 2 depicts a schematic picture of the procedure. First of all, cross-linker, PTMG and in some cases, mPEG with a desired stoichiometry ratio of NCO to OH group is packed into a simulation box. The system was energy minimized using a steep integrator and then equilibrated at 27 °C and atmospheric pressure with 10 fs time step for 50 ns under *NPT* conditions. Temperature was controlled by the modified Berendsen thermostat while for the pressure the Parrinello–Rahman barostat was used with P = 1 bar and τ_p = 3 ps. In order to follow the NCO and OH beads that have a probability of forming urethane bonds, the program selects one snapshot of the relaxation trajectory (at 80% of the total duration of this step). We employed a stepwise protocol to form the chemical bond between NCO and OH beads by using a determined reaction distance of d_R = 0.4 ± 10% nm (reaction cut-off).[20] This value, 0.4 nm ± 10%, is almost the smallest cut-off distance we could consider. For a cut-off distance smaller than 0.4 nm, *e.g.*, 0.35 nm, almost no potential reactant beads are found within the cut-off distance. For a cut-off distance of 0.45 nm, the final conversion and end-group index are 96.6% and 0.167, respectively, and hence do not change dramatically. For still larger values, the number of new bonds formed in one reaction loop is so high that it may impose high energy penalties. After finding NCO and OH beads within the cut-off distance, the program modifies the structure file by changing the bead types to the resulting urethane beads, namely, UNCO and UOH. It is worth emphasizing that in cases with more than one possible urethane bond formation for an NCO or an OH bead, only one bond formation is allowed, as occurs in real chemical reactions. Moreover, after the formation of a urethane bond, the corresponding bonded potential information is added to the bond section of the topology file and consequently, the additional angle potentials are determined and added to the angle list as well. After creating new bonds, the program performs a simulation to relax the system with 0.5 fs time step for 5 ns before a new bond creation is carried out. This relaxation part was carried out under similar conditions as stated before. Note that all steps of this procedure are carried out at the same temperature. The program repeats this loop of action until no reaction occurs during 100 consecutive cycles. As explained before, every reaction simulation is followed by a considerably longer relaxation simulation in which no reaction takes place. Therefore, due to the dynamics of the system,

Table 1 Comparison of density, radius of gyration and end-to-end distance values at AA and CG levels. The densities are measured at 25 °C and the R_gs and R_{end}s are measured at 27 °C

	Density (g cm^{-3})			Radius of gyration (Å)		End-to-end distance (Å)	
	Experimental	Atomistic	CG MARTINI	Atomistic	CG MARTINI	Atomistic	CG MARTINI
Cross-linker	1.14[a]	1.06	0.986	5.80	5.84	—[e]	
PTMG	0.978[b]	0.993	1.006	8.48	8.52	22.66	23.42
mPEG	1.089[c]	1.099	1.162	6.73	6.72	16.12	16.75
n-Butyl acetate	0.882[d]	0.897	0.841	—		—	

[a] T = 20 °C. [b] T = 25 °C, M = 650 g mol^{-1}. [c] T = 25 °C, M = 550 g mol^{-1}. [d] T = 20 °C. [e] For non-linear structure end-to-end distance is not defined.

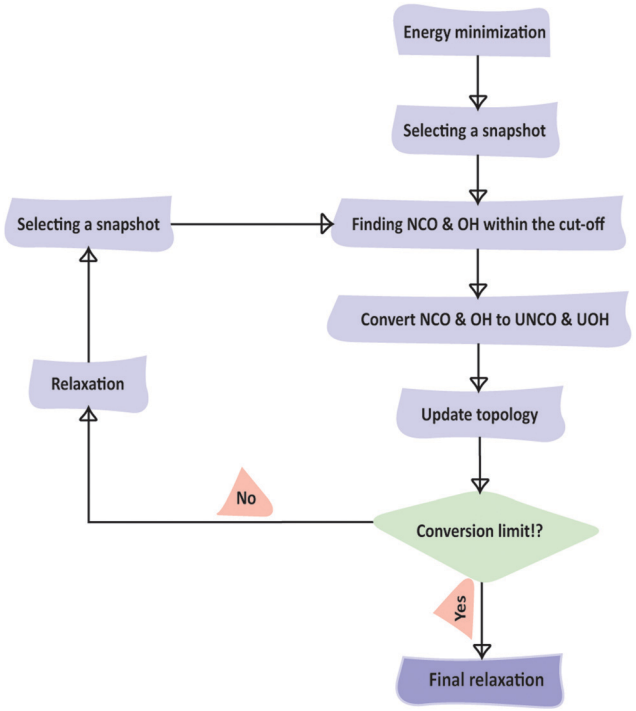

Fig. 2 Schematic of the procedure of the polymerization algorithm.

reacting beads might fall into the reaction cut-off distance and escape from it several times before they react, meaning that the reaction rate constant is not infinite.

The real reaction condition is not as simple as explained. In fact, most molecular simulations consider the simplest reaction conditions to study cross-linking, *e.g.*, addition of the stoichiometric ratio of reactants at a constant temperature in the absence of solvent. In our model, we step up closer to the real, and more complicated, conditions and we developed this method in such a way that it is capable of introducing a solvent at different stages of the reaction as well as evaporating solvent with different rates. Moreover, this method is able to alter the sequence of addition of materials, *e.g.*, diol, dangling chains, cross-linker, and solvent molecules, to the reaction. Therefore, we designed several case studies to evaluate the effect of various reaction parameters on the evolution of the network structure, see Table 2.

Besides doing the cross-linking reaction simulation, it is also very important to have a sophisticated set of analyses to study the effect of each reaction parameter on the final structure of the network. In fact, CG-MD simulations give detailed information about the position and connectivity of beads in time. We combine this information with graph theory to obtain valuable information about the network structure during cross-linking under different conditions. In this way, we designed a size exclusion characterization (SEC) rather similar to size-exclusion chromatography to study the evolution of the network as cross-linking proceeds. We also defined an end-group index from the population of beads with different connectivity to obtain information about the network structure. Since the core of the cross-linker, *i.e.*, the NCC bead, does not react and the number of them remains constant, it is the only bead with connectivity three. Therefore, we defined the end-group index as is given in eqn (1):

$$i_{\text{end}} = \frac{N_1}{N_3} \quad (1)$$

where N_1 and N_3 represent the number of beads with connectivity one and the number of NCC beads, respectively. It is worth emphasizing that the polymeric chains that are not connected to the network from both sides are considered as defects in the network. The end-group index is defined to quantify the number of defects in the network. For an ideal network without any dangling chain, this end-group index will be zero and the closer the end-group index is to zero, the denser polymeric network is obtained.

Other physical properties, such as shrinkage and the glass transition temperature T_g, are also studied. The shrinkage is calculated by keeping track of the density as a function of conversion and T_g is estimated by a set of "dilatometry simulations" in which the material is heated up and cooled down in a cycle and the volume-temperature graph is plotted. The temperature at which a distinct change in slope in the cooling curve occurs is taken as T_g. Full details of these calculations are covered in the ESI,† Section S3.

In the next section, after verifying our method and establishing our analysis techniques, we present the network structure of various cases mentioned in Table 2 and thereafter compare some physical properties of these structures.

3. Results and discussion

3.1. Method verification

In this section, we analyze different properties of PU systems as a function of reaction time (conversion) in order to verify our method. For this purpose, we only study PU systems without mPEG dangling chains, *i.e.*, cases I, II and III in Table 2. Therefore, we studied the structure and properties of the three mentioned PU systems under different reaction conditions, *i.e.*, (a) stoichiometric reaction at 25 °C, (b) stoichiometric reaction at 100 °C and (c) 5% excess of NCO groups at 100 °C. The other cases are covered in the next sections. Note that we continue the reaction until during 100 consecutive reaction loops, see Fig. 2, no further reaction takes place.

It is often tricky to carry out quantitative analysis on the effect of reaction parameters on the evolution of cross-linking conversion in experiments. However, such a study is rather straightforward in simulations due to the availability of all bead information in every single snapshot. Fig. 3 illustrates the reaction conversion as a function of reaction time. The conversion calculation is based on the limiting reactant (OH groups) and the reaction time is introduced in arbitrary units since our method is based on a CG model in which the interactions are rather smoother than atomistic simulations so that the time scale associated with the dynamics is (somewhat) uncertain. As shown, the increase of the conversion slows down with reaction time for all cases with two distinct regimes present: one for

Table 2 Materials and reaction conditions of all case studies

Case		Number of molecules: Cross-linker	PTMG	mPEG	nBAc	NCO/OH	Cross-linking Temp. [°C]	Solvent evaporation	Theoretical gel point [%]
I		500	750	—	3620	1/1	25	No	70.7
II		500	750	—	3620	1/1	100	No	70.7
III		525	750	—	3692	1.05/1	100	No	72.5
IV		500	685	130	3810	1/1	100	No	74.0
V	Step1	500	—	130	3810	1/1	100	No	74.0
	Step2	—	685	—	—				
VI	Step1	500	—	130	3810	1/1	100	Yes	74.0
	Step2	—	685	—	—				

smaller conversions, *i.e.*, up to about 70%, and one for larger conversions, *i.e.*, from about 70% upward, as highlighted in Fig. 3. Similar trends have been observed for many cases in simulations[33,69] and experiments.[70,71] Moreover, the conversion proceeds faster at a higher temperature, *i.e.*, case II as compared to case I. It is worth noting that the typical experimental reaction temperature for similar systems is around 100 °C. The increase in reaction rate is rationalized by the higher mobility of polymer segments at higher temperature which results in a higher chance of finding OH and NCO groups within the reaction cut-off distance at a certain number of reaction cycles. The effect of temperature is more pronounced in the second regime such that the conversion does not exceed 93% for case I by applying the final reaction time criterion. It is also shown that an excess amount of NCO, case III, results in a higher conversion value in the second regime, see Fig. 3. This is due to the improved access of OH to NCO groups in case III where 5% excess amount of NCO is provided.

It is interesting to visualize the growth of the polymer network as the reaction proceeds; however, this is not often possible for experiments due to technical complexities, particularly in the case of thermoset systems. Thus, the route through which the network evolves is not very clear. We have identified the largest polymer cluster by mapping the connectivity of beads and tracked the evolution of this cluster as conversion increases. Fig. 4 shows the growth of the molecular weight of this cluster as a function of conversion. As clearly shown, three regimes exist for the evolution of this cluster. In the first regime, *i.e.*, up to 65–70% conversion, the size of the cluster does not grow considerably. From this conversion on, rapid growth can be observed; therefore, in the second regime, *i.e.*, from around 70% to 90% conversion, a "cluster rapid expansion" takes place. The growth slows down again in the final regime of the reaction, *i.e.*, from 90% to the final conversion. It is interesting that the first regime change in the network growth coincides with the abrupt decrease in the reaction rate, see Fig. 3. This coincidence is due to the sudden growth of the cluster size in which the availability of reactive functional groups considerably decreases. This results in a lower probability of finding reactive groups within the reaction cut-off distance and therefore a lower reaction rate. In other words, it seems that up to 65–70% conversion smaller clusters are forming in the box. After 70% conversion, these small clusters start to connect to each other and this leads to the size expansion of the cluster in the second regime. As conversion proceeds higher than 90%, *i.e.*, the third regime, although the conversion increases, most of the reactions between OH and

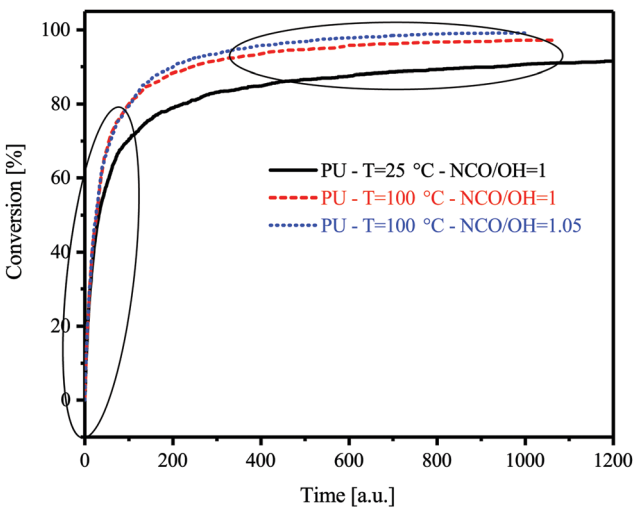

Fig. 3 Conversion as a function of reaction time for cases I, II and III.

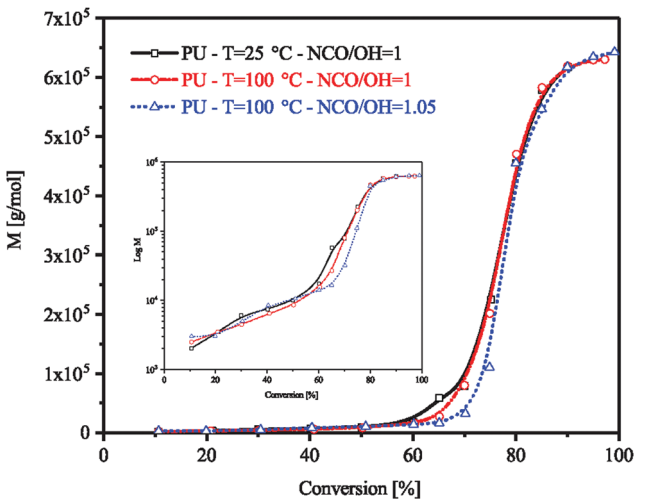

Fig. 4 Molecular weight of the largest cluster (M) as a function of conversion for cases I, II and III. Inset shows the log M *vs.* conversion. The lines are splines and a guide for the eye.

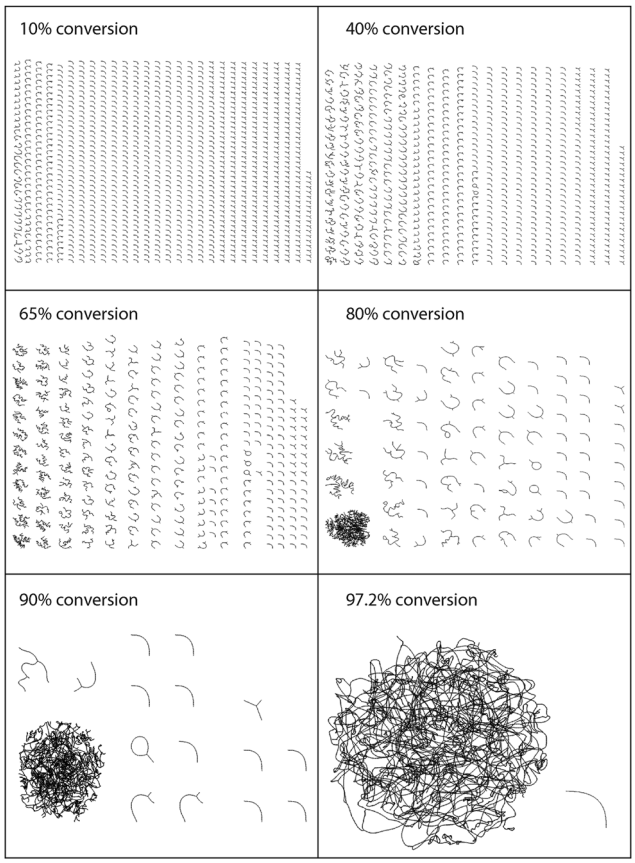

Fig. 5 Molecular structure for case II at 10%, 40%, 65%, 80%, 90% and 97.2% conversion. The beads and bonds are plotted with equal size and length, respectively. The bead positions are changed arbitrarily to achieve the best representation.

NCO groups occur inside the cluster such that the cross-link density increases largely while the size of the cluster does not increase much. This evolution behavior of the largest clusters is in good agreement with results from other research.[30,72]

The hypothesis described above requires more concrete proof; therefore, we performed another analysis by using the connectivity information of the beads and employing the Matlab graph and network algorithm library to visualize the evolution of the molecular structure of the system. Combining these tools operates like size-exclusion chromatography: it identifies each cluster in the system and sorts all clusters based on the number of beads that belong to them, *i.e.*, the size of the cluster. Fig. 5 shows the result of such analysis for 10%, 40%, 65%, 80%, 90% and the final conversion for case II. As shown, the size of clusters does not grow significantly from 10% to 65% conversion. The small clusters start to connect to each other from 65–70% onwards so that the number of small clusters has dropped rapidly at 80% conversion and most of the unconnected ones have joined the largest cluster in the regime up to 90% conversion. From then on, the size of the main cluster does not change much; however, the population of connecting bonds increases in number substantially.

It intrigued us that the abrupt change in the reaction rate, size, and structure growth of the network occurs at about 70% conversion. Looking back at Table 2, we calculated and reported theoretical gel points of all cases based on eqn (2):[73]

$$p_c = \frac{1}{\{r(f_{w,A}-1)(f_{w,B}-1)\}^{\frac{1}{2}}}, \quad f_{w,A} = \frac{\sum {f_{A_i}}^2 N_{A_i}}{\sum f_{A_i} N_{A_i}}, \quad f_{w,B} = \frac{\sum {f_{B_j}}^2 N_{B_j}}{\sum f_{B_j} N_{B_j}} \quad \text{and} \quad r = \frac{\sum f_{A_j} N_{A_j}}{\sum f_{B_j} N_{B_j}} \tag{2}$$

where p_c is the conversion at the gel point and $f_{w,A}$ and $f_{w,B}$ are weight-average functionalities of the OH and NCO functional groups, respectively. The parameter r describes the stoichiometric imbalance (molar ratio of an OH functional group to NCO functional group), f_A and f_B represent the functionalities of the diol and cross-linker molecules, while N_A and N_B are the numbers of diol and cross-linker molecules. For cases I and II the gel point occurs at 70.7% conversion while this point is at 72.5% conversion for case III. As is evident from Fig. 4, the initiation of the cluster size expansion for the three cases follows a similar trend but takes place at slightly larger conversion for case III as compared to the other cases. This is, indeed, another important verification for our model.

Apart from predicting the network structure, one expects a model to predict some physical properties of the network as well. We calculated the shrinkage and T_g of the material as cross-linking proceeds and plotted the results in Fig. 6a and b, respectively. As expected, the total volume of the material decreases because of cross-linking with a total density increase of 1.41%. T_g as a function of conversion shows a logical trend. It increases more-or-less linearly with the conversion from about −20 °C to 43 °C. This expected increase in T_g can be explained by two mechanisms, *i.e.*, (a) as cross-linking proceeds, the cooperative movements of polymer segments (beads) become more limited due to the new bond formations and (b) the newly formed urethane groups strengthen the molecular interactions by forming hydrogen bonds.[9] We also calculated the mean squared displacement of the beads as a function of conversion and a more-or-less linear decay is observed, see the ESI,† Section S4. Thus, a linear increase in T_g with conversion is a reasonable trend one would expect.

After examining our method capabilities for simpler systems, *i.e.*, cases I, II and III, we focus now on more complex systems in which mPEG dangling chains are present and on more complicated and realistic reaction conditions, *e.g.*, including the evaporation of the solvent.

3.2. Effect of dangling chains

In this section, we study the PU systems in which dangling chains are present. We use mPEG dangling chains that can react to NCO groups from one side of the chain, see Fig. 1. As mentioned earlier, the distribution of dangling chains in the network is of great importance. Besides, the effect of incorporation of such chains and also the sequence of addition of them can affect the physical properties of the PU network. Therefore, we consider three case studies, *i.e.*, cases IV, V and VI, in order to show the ability of our method in addressing such issues.

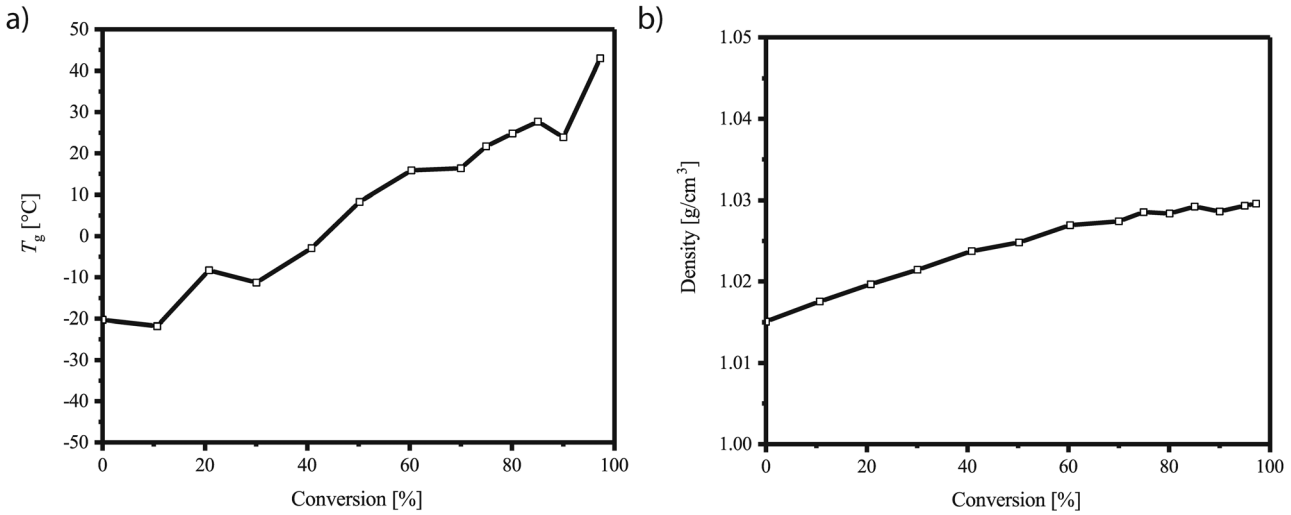

Fig. 6 (a) T_g as a function of conversion and (b) cross-linking shrinkage for case II. The lines connect the measured data points and are a guide for the eye.

As summarized in Table 2, we added mPEG chains together with other reactants in a single step, at the beginning of the reaction, for case IV while for cases V and VI, we, first, mixed mPEG, cross-linker, and solvent at the first step of the reaction and after almost all mPEG chains reacted with the cross-linkers, we added diols to the reaction. For case V, the reaction takes place in the solvent; however, for case VI, the second step starts with a similar solid content but the solvent gradually evaporates in such a way that after 100 simulation loops the solvent is completely evaporated. We used a linear function of time to remove solvent molecules from the box. To avoid the use of μVT conditions, in each loop only 38 solvent molecules (114 beads) were removed from the system, amounting to only about 0.37% of all beads present in the box. After removing the solvent molecules, the topology files were updated automatically by a simple script and a relaxation step was carried out. This means that in each loop the number of molecules was constant (thus rendering NVT conditions applicable), although it was lower than in the previous loop. Fig. 7 shows the conversion-time graph and final conversions of these three cases. At first sight, the difference between case IV and the two other cases is obvious. In the latter cases, at 8.6% conversion, all mPEG chains are reacted and after addition of diol chains, the reaction rate shoots up again and reaches a plateau close to the final conversion for case IV. This indicates that the sequence of addition does not influence the final conversion. However, case VI resulted in a larger conversion as compared to the other ones. The only difference between cases V and VI is the evaporation of the solvent. In fact, case VI resembles the real reaction condition for coating applications in which after addition of diol, the mixture is applied on a substrate and evaporation and curing starts at this point. A comparison between the conversion growth of these cases shows that the evaporation of solvent accelerates the reaction between OH and NCO groups. It is worth emphasizing that this acceleration begins at around the gel point while before that point is reached, the reaction rates

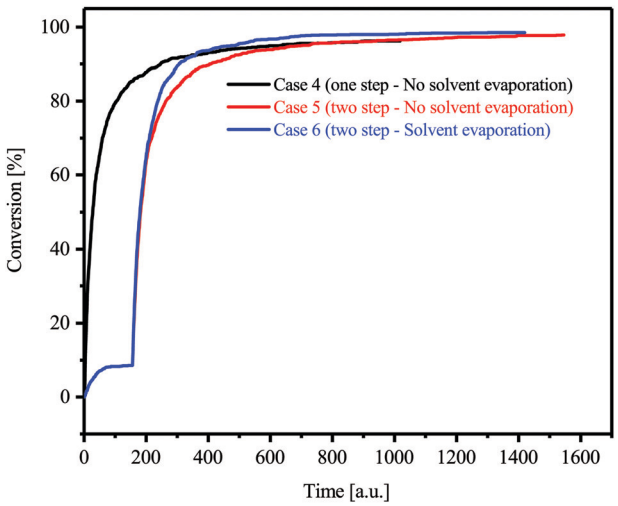

Fig. 7 Reaction conversion as a function of simulation cycles for cases IV, V and VI.

are similar for both cases although the evaporation has been already started. We rationalize this observation by the fact that the presence of solvent molecules facilitates the movement of small species and at the same time, leads to network swelling. The swelling of the network by the solvent is a result of non-bonded Martini interactions between polymer and solvent beads. Swelling depends on the overall balance between attractive and repulsive beads. Overall, we obtained attractivity for the solvent so that it is miscible with all prepolymers and it can swell the network homogeneously, as confirmed by analyzing the density profile of the solvent during simulations. At the gel point, the clusters start connecting to each other, as discussed later, and therefore after this point the reacting beads need to take much longer paths to find another reacting partner. The solvent swells the network and makes this path even longer. Moreover, evaporation of solvent molecules leads to

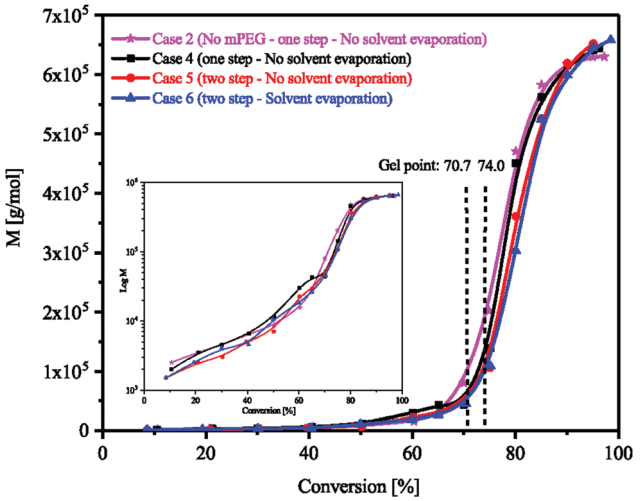

Fig. 8 Molecular weight of the largest cluster (M) as a function of conversion for cases II, IV, V and VI. Inset shows the log M *vs.* conversion. The lines are splines and a guide for the eye.

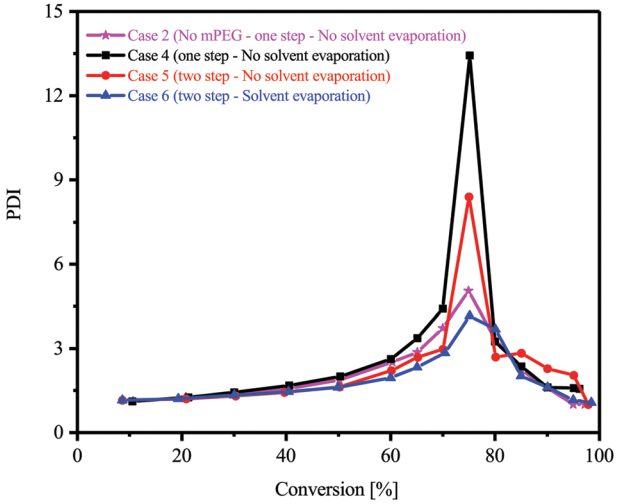

Fig. 9 Polydispersity index (PDI) of all clusters except the largest one as a function of conversion. The lines are splines and a guide for the eye.

molecular-sized cavities in the system that gives more freedom to beads to search for reacting partners during shrinkage of the system. Nevertheless, at much longer reaction time, the conversion for all cases becomes almost similar.

We illustrate the molecular weight of the largest cluster for cases II, IV, V, and VI in Fig. 8. The trend emphasizes that the onset of the sudden growth of the molecular weight of the largest cluster occurs at the theoretical gel point, similar to what we observed in Fig. 4. The small shift of onset points for cases IV, V and VI as compared to case II reconfirms the reliability of our model since their theoretical gel point is slightly higher, see Table 2. The three regimes observed for the previous cases are still present for mPEG containing PU systems. The rate by which the largest cluster grows in the second regime for cases V and VI is more-or-less similar and slightly slower as compared to case IV and II. Despite the higher reaction rate for case VI as compared to case V between 70% and 90% conversions, see Fig. 7, the largest cluster grows with a more-or-less similar rate for all these cases in this regime. We expect that the aforementioned higher reaction rate is due to the reactions taking place either between and within smaller clusters or within the largest cluster. Thus, although more reactions between OH and NCO groups take place for case VI in this regime, the size of the largest cluster is not influenced. Therefore, during solvent evaporation, a smaller number of clusters and a more uniform cluster size are expected.

We studied the size and size distribution for other clusters in the system in order to examine our hypothesis. We skipped the largest cluster and measured the number and weight average molecular weight, *i.e.*, M_n and M_w, of the other clusters in the system at different conversions. Then we calculated their polydispersity index (PDI), as a measure of the cluster size distribution, see eqn (2), and plotted these values as a function of conversion in Fig. 9. Note that M_n and M_w values are tabulated in the ESI,† Section S5. As shown, the PDI values for all cases show a peak around the gel point. The lower the height of the peak, the more uniform cluster size distribution exists. As is apparent, the height of the PDI peak is considerably lower at the gel point for case VI as compared to case V. These results also indicate that two-step addition of material considerably lowers the cluster size distribution so that the highest PDI value at the gel point belongs to case IV.

Apart from the evolution of cross-linking reactions, the final structure of the material made under certain conditions is of great importance. We believe that the presence of mPEG dangling chains, sequence of addition and solvent evaporation influence the final structure and therefore properties of PU systems. Our analysis method makes it fairly easy to study the structure and properties of the cross-linked material individually and this paves the way for structure–property analysis of such systems. For the sake of an example, we use our simulated SEC to illustrate the final structure of PU made for cases II, IV, V and VI. As shown in Fig. 10, different final structures arise despite the very similar final conversion, see Table 3. Obviously, one-step addition of material to the reaction, *i.e.*, case IV, leads to a considerable number of unreacted species in the final stage. It is worth noting that the linear small chains with red color are mPEG dangling chains. By splitting the reaction into two steps, no unreacted mPEG remains at the end of the reaction and this emphasizes the successfulness of the two-step-addition strategy over one-step-addition. This can be seen in Fig. 10 obviously, for case IV, that 15.4% of mPEG dangling chains did not participate in the largest cluster. Based on our visualizations, almost each mPEG chain, reacted with a separate cross-linker molecule in the two-step addition while this is not the case for a one-step route. For case VI, despite the two-step addition of material, some larger clusters are unable to connect to the main cluster at the end. It is worth emphasizing that exactly similar simulation boxes are used for the second step of simulation for cases V and VI. One also observes the formation of loops in the system under solvent evaporation conditions, which are often considered as defects in the network structure.

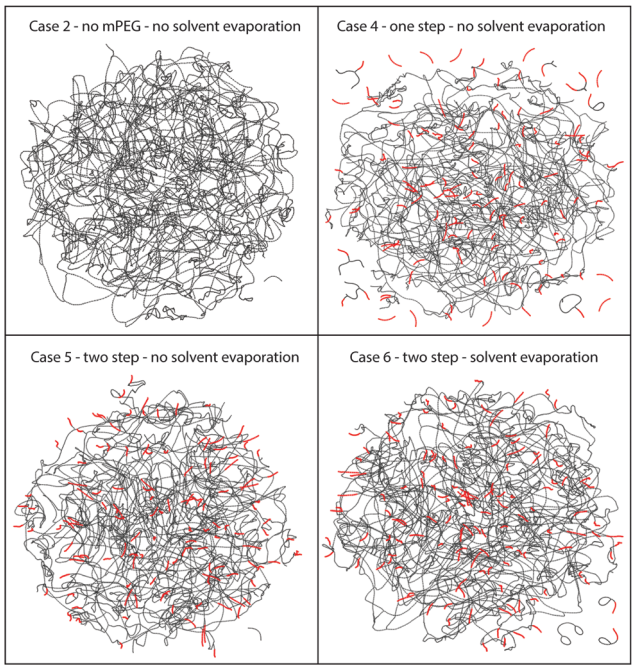

Fig. 10 Molecular structure for cases II, IV, V and VI at final conversion. The beads and bonds are plotted with equal size and length, respectively. The bead positions are changed arbitrarily to achieve the best representation. Black lines show the PU network and the red ones show the mPEG dangling chains.

Table 3 Final conversion, i_{end} and T_g of cases II, IV, V and VI. The values are obtained as the average of at least three independent simulations

	Final conversion	End-group index	T_g (°C)
Case II	97.20 ± 0.25	0.164 ± 0.012	41.3 ± 4.6
Case IV	96.19 ± 0.25	0.413 ± 0.007	26.3 ± 2.3
Case V	97.86 ± 0.25	0.384 ± 0.011	25.1 ± 6.3
Case VI	98.46 ± 0.16	0.351 ± 0.010	27.7 ± 2.0

Looking back at Fig. 10, similar network structures for the final conversion of case II, *i.e.* PU with no dangling chains, and case V, *i.e.*, PU with mPEG dangling chains made by the two-step addition of material, are obtained. However, introducing mPEG dangling chains to the reaction makes a clear difference in the network structure, that is, it introduces a considerable population of end groups (beads with one connectivity, in the network). In fact, our simulated SEC is not only capable of separating different clusters but is also capable of studying the structure of each individual cluster as well. For instance, it can find the population of beads with a certain number of connectivity in one cluster. Therefore, we defined the end-group index, *i.e.*, i_{end}, that reflects the normalized population of end groups in the system, see Section 2.4. This index, however, is not a reliable measure up to conversions in which the size difference between the largest clusters and the other ones is not significant. Note that up to 40% conversion, there is no main cluster such that the cluster we chose as the largest one is not the same from one conversion to the other. Therefore, up to this point, this index does not belong to a specific cluster.

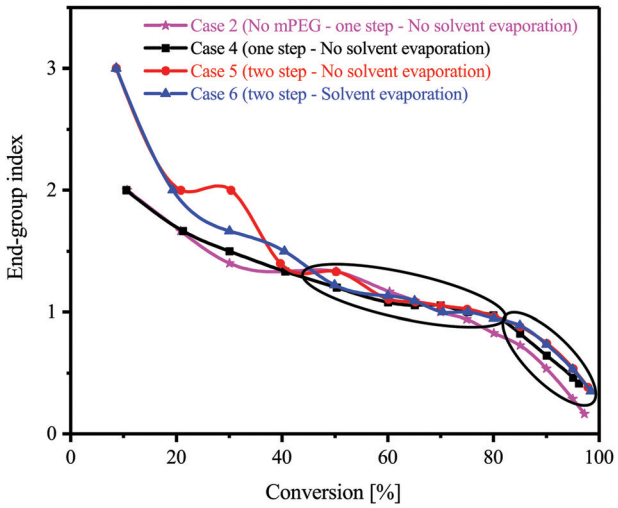

Fig. 11 End-group index as a function of conversion for cases II, IV, V and VI. The lines are splines and a guide for the eye.

Thus, we only elaborate on the results obtained above this conversion limit. As shown in Fig. 11, there are two distinct regimes visible for this index, *i.e.*, a slow and fast decay. In fact, as the reaction proceeds, the number of beads with connectivity one in the largest cluster decreases. Above about 85% conversion, this decay accelerates which is another clarification of the mechanism we illustrated in Section 3.1. Before this conversion, the largest cluster was adding smaller clusters to itself and from this point on, most of the reactions take place inside the cluster, therefore, as one reaction takes place, two end groups disappear. Moreover, the decay in this regime is relatively large for case II as compared to the cases including mPEG chains. This, of course, is because mPEG chains can only react from one side and they add one permanent end group to the PU system.

As the final step of our analysis, we measured the T_g of PU networks made in different cases. We used the same protocol as used in the previous section and explained in the ESI,† Section S3, for all T_g calculations. As indicated in Table 3, T_g drops by addition of mPEG to PU systems, a common observation when dangling chains are included. Considering the fact that mPEG and PTMG chains have more-or-less similar stiffness, as both show a similar characteristic ratio,[74] the decrease in T_g could be rationalized by the mPEG end groups added to the system. These end groups provide free volume to the system and result in a lower T_g. This effect can be reconfirmed by comparing the final end-group indices in Table 3. This index is rather similar for all cases with mPEG and considerably smaller for case II in which no dangling chain presents. Note that the final conversion of all cases is rather similar.

Based on our visualization analysis, the reaction conditions under which mPEG chains are added to the system do not considerably influence the nano-phase separation of the hard and soft segments. We also noticed some degree of nano-phase separation between PTMG and mPEG chains under all reaction conditions; however, the two-step reaction shows a slightly more homogeneous distribution of dangling chains. The pictures are provided in the ESI,† Section S6.

4. Conclusions

A comprehensive MD method for step-growth polymerization based on the CG MARTINI model is developed and tested on thermoset PU systems. Our MD method is implemented in a fully automated manner and is capable of updating necessary topological information during the reaction. The method is also able to mimic realistic reaction conditions, such as solvent evaporation and changing the sequence of addition of materials to the reaction. We also designed and developed several analytical methods in order to analyze the results of this model for a better understanding of the effect of reaction conditions on PU network structures. We presented a simulated SEC test by which we obtained insight into the mechanisms of the cross-linking reactions in the different conversion regimes. We used two structural indices and by combining them, we were able to substantiate our hypothesis about the network evolution during cross-linking. In fact, we believe that at the beginning of the reaction, smaller clusters are formed and as the reaction proceeds, they start to connect to each other and form a large cluster. The increase in cluster size coincides with the theoretical gel point, where the reaction rate relatively suddenly drops. After this increase in the size of the main cluster, the reaction of the cross-link point occurs in such a way that above 90% conversion the size of the cluster is almost constant and from that point on, the reactions mainly take place between reactive groups within the main cluster.

We also studied the incorporation of mPEG dangling chains to the PU network. Based on our simulations, a two-step addition of material, *i.e.*, first a mixing and reacting step of the mPEG chains with the cross-linker and second the addition of PTMG as a diol, meanwhile keeping the solvent in the network during the reaction, leads to the most integrated network. We also performed some MD simulations on the network structures made under different reaction conditions and we noticed, as expected, that the incorporation of mPEG dangling chain lowers the T_g, but also that different reaction routes might lead to different physical properties despite having the same conversion.

Conflicts of interest

There are no conflicts to declare.

Acknowledgements

This work was supported by a travel grant of the Iranian Ministry of Science, Research and Technology.

References

1 B. John, in Handbook of Polymernanocomposites, *Processing, Performance and Application*, Springer, 2014, pp. 341–359.
2 D. Shen, S. Shi, T. Xu, X. Huang, G. Liao and J. Chen, *Constr. Build. Mater.*, 2018, **174**, 474–483.
3 M. Szycher, *Szycher's handbook of polyurethanes*, CRC press, 1999.
4 J. Li, L. Ma, G. Chen, Z. Zhou and Q. Li, *J. Mater. Chem. B*, 2015, **3**, 8401–8409.
5 N. K. Lamba, *Polyurethanes in biomedical applications*, Routledge, 2017.
6 X. Lu, S. Romero-Vargas Castrillón, D. L. Shaffer, J. Ma and M. Elimelech, *Environ. Sci. Technol.*, 2013, **47**, 12219–12228.
7 B. S. Kim, J. S. Hrkach and R. Langer, *Biomaterials*, 2000, **21**, 259–265.
8 Q. Tian, G. Yan, L. Bai, X. Li, L. Zou, L. Rosta, A. Wacha, Q. Li, I. Krakovský, M. Yan and L. Almásy, *Polymer*, 2018, **147**, 1–7.
9 H. Makki, K. N. Adema, E. A. Peters, J. Laven, L. G. van der Ven, R. A. van Benthem and G. de With, *J. Polym. Sci., Part B: Polym. Phys.*, 2016, **54**, 659–671.
10 P. Schön, K. Bagdi, K. Molnár, P. Markus, B. Pukánszky and G. J. Vancso, *Eur. Polym. J.*, 2011, **47**, 692–698.
11 J. Goclon, T. Panczyk and K. Winkler, *Appl. Surf. Sci.*, 2018, **433**, 213–221.
12 G. Kacar, P. T. Albers and A. C. C. Esteves, *J. Coat. Technol. Res.*, 2018, **15**, 691–701.
13 J. Repáková, P. Čapková, M. Studenovský and M. Ilavský, *J. Mol. Model.*, 2004, **10**, 240–249.
14 Y. Lan, D. Li, J. Zhai and R. Yang, *Ind. Eng. Chem. Res.*, 2015, **54**, 3563–3569.
15 E. Iype, A. Esteves and G. de With, *Soft Matter*, 2016, **12**, 5029–5040.
16 A. Esteves, K. Lyakhova, L. van Der Ven, R. van Benthem and G. de With, *Macromolecules*, 2013, **46**, 1993–2002.
17 Y. Zhang, F. Karasu, C. Rocco, L. van der Ven, R. van Benthem, X. Allonas, C. Croutxé-Barghorn, A. Esteves and G. de With, *Polymer*, 2016, **107**, 249–262.
18 J. Hu, C. Zhang, X. Li, J. Han and F. Ji, *Polym. Chem.*, 2017, **8**, 260–271.
19 Z. Pan, L. Yu, N. Song, L. Zhou, J. Li, M. Ding, H. Tan and Q. Fu, *Polym. Chem.*, 2014, **5**, 2901–2910.
20 H. Makki, K. N. Adema, E. A. Peters, J. Laven, L. G. van der Ven, R. A. van Benthem and G. de With, *Polym. Degrad. Stab.*, 2014, **105**, 68–79.
21 A. Vashisth, C. Ashraf, W. Zhang, C. E. Bakis and A. C. van Duin, *J. Phys. Chem. A*, 2018, **122**, 6633–6642.
22 C. Wu and W. Xu, *Polymer*, 2006, **47**, 6004–6009.
23 K. S. Khare and R. Khare, *J. Phys. Chem. B*, 2013, **117**, 7444–7454.
24 K. S. Khare, F. Khabaz and R. Khare, *ACS Appl. Mater. Interfaces*, 2014, **6**, 6098–6110.
25 N. J. Soni, P.-H. Lin and R. Khare, *Polymer*, 2012, **53**, 1015–1019.
26 L. Gao, Q. Zhang, H. Li, S. Yu, W. Zhong, G. Sui and X. Yang, *Polym. Chem.*, 2017, **8**, 2016–2027.
27 P. V. Komarov, C. Yu-Tsung, C. Shih-Ming, P. G. Khalatur and P. Reineker, *Macromolecules*, 2007, **40**, 8104–8113.
28 N. Nouri and S. Ziaei-Rad, *Macromolecules*, 2011, **44**, 5481–5489.
29 C. Li, E. Jaramillo and A. Strachan, *Polymer*, 2013, **54**, 881–890.
30 V. Varshney, S. S. Patnaik, A. K. Roy and B. L. Farmer, *Macromolecules*, 2008, **41**, 6837–6842.

31 N. B. Shenogina, M. Tsige, S. S. Patnaik and S. M. Mukhopadhyay, *Macromolecules*, 2012, **45**, 5307–5315.
32 A. Bandyopadhyay, P. K. Valavala, T. C. Clancy, K. E. Wise and G. M. Odegard, *Polymer*, 2011, **52**, 2445–2452.
33 C. Li and A. Strachan, *Polymer*, 2010, **51**, 6058–6070.
34 H. Liu, M. Li, Z.-Y. Lu, Z.-G. Zhang, C.-C. Sun and T. Cui, *Macromolecules*, 2011, **44**, 8650–8660.
35 K. S. Khare and F. R. Phelan Jr, *Macromolecules*, 2018, **51**, 564–575.
36 A. A. Gavrilov, P. V. Komarov and P. G. Khalatur, *Macromolecules*, 2014, **48**, 206–212.
37 D. R. Heine, G. S. Grest, C. D. Lorenz, M. Tsige and M. J. Stevens, *Macromolecules*, 2004, **37**, 3857–3864.
38 D. Doherty, B. Holmes, P. Leung and R. Ross, *Comput. Theor. Polym. Sci.*, 1998, **8**, 169–178.
39 M. K. Glagolev, A. A. Lazutin, V. V. Vasilevskaya and A. R. Khokhlov, *Polymer*, 2016, **86**, 168–175.
40 V. Y. Rudyak, A. A. Gavrilov, D. V. Guseva and A. V. Chertovich, *Macromol. Theory Simul.*, 2017, **26**, 1700015.
41 D. V. Guseva, V. Y. Rudyak, P. V. Komarov, A. V. Sulimov, B. A. Bulgakov and A. V. Chertovich, *J. Polym. Sci., Part B: Polym. Phys.*, 2018, **56**, 362–374.
42 M. S. Radue, V. Varshney, J. W. Baur, A. K. Roy and G. M. Odegard, *Macromolecules*, 2018, **51**, 1830–1840.
43 G. Rossi, I. Giannakopoulos, L. Monticelli, N. K. Rostedt, S. R. Puisto, C. Lowe, A. C. Taylor, I. Vattulainen and T. Ala-Nissila, *Macromolecules*, 2011, **44**, 6198–6208.
44 H. Yagyu and T. Utsumi, *Comput. Mater. Sci.*, 2009, **46**, 286–292.
45 C. Li and A. Strachan, *J. Polym. Sci., Part B: Polym. Phys.*, 2015, **53**, 103–122.
46 G. Kacar, E. A. Peters and G. de With, *Comput. Mater. Sci.*, 2015, **102**, 68–77.
47 Y. Fu, J. Michopoulos and J.-H. Song, *Comput. Mater. Sci.*, 2015, **107**, 24–32.
48 G. S. Grest and K. Kremer, *Macromolecules*, 1990, **23**, 4994–5000.
49 P.-H. Lin and R. Khare, *Macromolecules*, 2009, **42**, 4319–4327.
50 S. J. Marrink, H. J. Risselada, S. Yefimov, D. P. Tieleman and A. H. de Vries, *J. Phys. Chem. B*, 2007, **111**, 7812–7824.
51 S. J. Marrink, A. H. de Vries and A. E. Mark, *J. Phys. Chem. B*, 2004, **108**, 750–760.
52 D. H. de Jong, G. Singh, W. D. Bennett, C. Arnarez, T. A. Wassenaar, L. V. Schäfer, X. Periole, D. P. Tieleman and S. J. Marrink, *J. Chem. Theory Comput.*, 2012, **9**, 687–697.
53 F. A. Herzog, L. Braun, I. Schoen and V. Vogel, *J. Chem. Theory Comput.*, 2016, **12**, 2446–2458.
54 L. Monticelli, S. K. Kandasamy, X. Periole, R. G. Larson, D. P. Tieleman and S. J. Marrink, *J. Chem. Theory Comput.*, 2008, **4**, 819–834.
55 C. A. López, A. J. Rzepiela, A. H. de Vries, L. Dijkhuizen, P. H. Hünenberger and S. J. Marrink, *J. Chem. Theory Comput.*, 2009, **5**, 3195–3210.
56 J. J. Uusitalo, H. I. Ingólfsson, P. Akhshi, D. P. Tieleman and S. J. Marrink, *J. Chem. Theory Comput.*, 2015, **11**, 3932–3945.
57 J. J. Uusitalo, H. I. Ingólfsson, S. J. Marrink and I. Faustino, *Biophys. J.*, 2017, **113**, 246–256.
58 J. Zavadlav, M. N. Melo, A. V. Cunha, A. H. de Vries, S. J. Marrink and M. Praprotnik, *J. Chem. Theory Comput.*, 2014, **10**, 2591–2598.
59 G. Rossi, L. Monticelli, S. R. Puisto, I. Vattulainen and T. Ala-Nissila, *Soft Matter*, 2011, **7**, 698–708.
60 S. Nawaz and P. Carbone, *J. Phys. Chem. B*, 2014, **118**, 1648–1659.
61 P. Banerjee, S. Roy and N. Nair, *J. Phys. Chem. B*, 2018, **122**, 1516–1524.
62 R. G. Uttarwar, J. Potoff and Y. Huang, *Ind. Eng. Chem. Res.*, 2012, **52**, 73–82.
63 H. J. Berendsen, D. van der Spoel and R. van Drunen, *Comput. Phys. Commun.*, 1995, **91**, 43–56.
64 M. Vögele, C. Holm and J. Smiatek, *J. Mol. Liq.*, 2015, **212**, 103–110.
65 M. Vögele, C. Holm and J. Smiatek, *J. Chem. Phys.*, 2015, **143**, 243151.
66 J. Michalowsky, L. V. Schäfer, C. Holm and J. Smiatek, *J. Chem. Phys.*, 2017, **146**, 054501.
67 J. Michalowsky, J. Zeman, C. Holm and J. Smiatek, *J. Chem. Phys.*, 2018, **149**, 163319.
68 H. Lee, A. H. de Vries, S.-J. Marrink and R. W. Pastor, *J. Phys. Chem. B*, 2009, **113**, 13186–13194.
69 C. Li and A. Strachan, *Macromolecules*, 2011, **44**, 9448–9454.
70 R. B. Prime, C. Michalski and C. M. Neag, *Thermochim. Acta*, 2005, **429**, 213–217.
71 S. Turri, T. Trombetta and M. Levi, *Macromol. Mater. Eng.*, 2000, **283**, 144–152.
72 C. Li and A. Strachan, *Polymer*, 2011, **52**, 2920–2928.
73 G. Odian, *Principles of polymerization*, John Wiley & Sons, 2004.
74 C. G. Richardson, *Doctor of Philosophy*, Loughbrough University of Technology, 1971.

